Synthesis, characterization and corrosion resistance of electroless nickel-phosphorus and nickel-phosphorus-SiC coatings: A comparative study

By M. Sc. Magali Camargo, Prof. Isabel Díaz, Lima, Dr. Udo Schmidt, Ilmenau and Prof. Andreas Bund, Ilmenau

Nickel-phosphorus and nickel-phosphorus-SiC coatings were obtained by electroless deposition processes using laboratory made and commercial nickel/hypophosphite based baths. The characterization techniques included scanning electron microscopy (SEM), glow discharge optical emission spectroscopy (GD-OES) and X-ray diffraction (XRD). All deposits showed an amorphous micro-structure and high phosphorus content. The incorporated SiC particles (2–5 µm) constituted about 10 wt.% of the composite deposits. The techniques used to study the corrosion resistance in 3.5 wt.% NaCl were linear polarization resistance (LPR), Tafel plots and electrochemical impedance spectroscopy (EIS). The results showed that nickel-phosphorus-SiC deposits experienced lower corrosion currents compared with the nickel-phosphorus coatings. This fact can be ascribed to the decrease in the effective surface area available for corrosion. Concerning the mechanism by which nickel-phosphorus and nickel-phosphorus-SiC deposits become corroded, through EIS experiments and Tafel plots, it was shown that the corrosion kinetics involved a charge transfer mechanism.

Nickel-Phosphor- und Nickel-Phosphor-SiC-Schichten wurden aus kommerziellen und im Labor angesetzten Elektrolyten abgeschieden. Die Schichten wurden mittels Rasterelektronenmikroskop (REM), Glimmentladungsspektroskopie (GD-OES) und Röntgenbeugung (XRD) untersucht. Alle Schichten zeigten eine amorphe Mikrostruktur und wiesen einen hohen Phosphorgehalt auf. Es wurden bis zu 10 Gew.% der Siliziumcarbidpartikel (2-5 mm) in die Schichten eingebaut. Für die Charakterisierung der Schichten wurde der Korrosionswiderstand in NaCl-Lösung (3,5 Gew.%) durch Bestimmung des linearen Polarisationswiderstandes (LPR), der Tafelkurven und der elektrochemischen Impedanz (EIS) ermittelt. Die Nickel-Phosphor-SiC-Schiten zeigten im Ergebnis einen geringeren Korrosionsstrom als Nickel-Phosphor-Schichten. Dies kann auf die geringere effektive Metalloberfläche für den Korrosionsangiff zurückgeführt werden. Im Zusammenhang mit den durchgeführten EIS- und Tafel-Messungen wurde festgestellt, dass bei beiden Schichtarten die Kinetik durch den Ladungstransfer bestimmt wird.

1 Introduction

Nowadays industrial sectors such as automotive, aerospace, electronics and textile increasingly require the use of materials with suitable properties for specific applications. One possibility to improve materials performance is to protect them by coatings.

Nickel-phosphorus (Ni-P) alloys obtained by electroless plating have contributed to a significant advance in the development of protective coatings because a nickel-phosphorus coating improves basis material properties such as corrosion resistance, hardness, wear resistance and surface uniformity [1, 2]. The addition of dispersed, hard micro/nano particles into the nickel-phosphorus matrix has led to the development of composite coatings. Nickel-phosphorus composite coatings exhibit an improved hardness and wear resistance. However, it is difficult to predict accurately their corrosion resistance because different parameters can influence the behavior of these coatings. In fact, the role of dispersed particles for the corrosion properties is still controversially discussed [3–5].

This research aims to synthetize, to characterize and to evaluate the corrosion resistance in NaCl 3.5% of as-plated nickel-phosphorus and nickel-phosphorus-SiC coatings with high phosphorus content. By using different electrochemical techniques a better understanding of the behavior of nickel-phosphorus and nickel-phosphorus-SiC can be achieved.

2 Experimental part

2.1 Synthesis of coatings

Electroless nickel-phosphorus and nickel-phosphorus-SiC deposits were obtained by electroless deposition using both lab made and commercial nickel/hypophosphite based baths. The chemical composition of the lab made plating bath consisted of:

- 30 g/L $NiSO_4 \cdot 7H_2O$
- 20 g/L $NaH_2PO_2 \cdot H_2O$
- 25 g/L lactic acid, 5 g/L propionic acid
- 1 mg/L Pb^{2+} (as $Pb(NO_3)_2$)

In the case of the plating baths used for the composite coatings, 25 g/L of SiC micro-sized particles (2–5 µm, *ESK*) were added to the original lab made and commercial baths. The pH value of all plating baths was adjusted to 4.8 with 5 M NaOH solution. All reagents were p.a. grade.

Low carbon steel panels (2.5 x 4.5 x 0.05 cm^3) were used as substrates. The pre-treatment of the substrates consisted of an electrolytic degreasing for 3 minutes at a current density of 6.5 A/dm^2 (cathodic mode) followed by a substrate pickling with HCl (1:1 v/v) for 3 minutes. Both procedures were done at room temperature.

In all the cases the plating was carried out by immersing the substrate into the electrolytic bath at 87 ± 1 °C immediately after the pre-treatment. The bath loading was 0.15 dm^2/L and the deposition time was 2 hours. In the case of nickel-phosphorus-SiC deposits, the electroless baths containing dispersed SiC particles were mechanically stirred at approx. 500 rpm with a two-bladed glass stirring element. The sample was vertically positioned and parallel oriented to the flow direction of the bath. After the deposition process the samples were rinsed with distilled water, dried and stored in a desiccator.

2.2 Characterization of deposits

The surface morphology of deposits was studied by scanning electron microscopy (SEM) using a *Philips XL 30* scanning electron microscope. The samples were examined in top and cross-sectional views.

The chemical composition of deposits was determined by GD-OES with a *GDA 750* spectrometer equipped with a DC source (1000 V, 13 mA). The diameter of the exposed sample area was 2.5 mm.

The microstructure of nickel-phosphorus and nickel-phosphorus-SiC deposits was studied by X-ray diffraction (XRD). An X-ray diffractometer (*Bruker AXS D 5000* operating with Cu-Kα radiation) with Goebel mirror was used. The studied sample area was approx. 1 cm^2. The method of study was grazing incidence diffraction [6].

The coatings thickness were determined by magnetic induction method and then verified by SEM in the surface cross-section of the samples. A *Deltascope MP30* (*Fischer*) thickness tester was used according with ASTM B 499-96 standard [7].

2.3 Evaluation of the corrosion resistance

All the electrochemical tests were performed using an *Autolab PGSTAT 302N* potentiostat/galvanostat equipped with a *FRA2* impedance module and controlled with the software *NOVA* version 1.4. The electrochemical tests used a conventional three-electrode electrochemical cell setup: the sample (nickel-phosphorus or nickel-phosphorus-SiC deposit) as the working electrode (WE), a silver/silver chloride electrode (Ag/AgCl 3M KCl) as the reference electrode (RE) and a platinum wire as the counter electrode (AE). The electrochemical cell consisted of a glass cylinder with a PTFE bottom plate with a hole in the center. The exposed sample area was 0.20 cm^2. All tests were carried out at room temperature.

The electrolytic solution was prepared by dissolving NaCl (p.a., *Merck*) in distilled water to give a concentration of 3.5 wt.%. In order to carry out tests with a constant concentration of oxygen in the salt solution, the electrolyte was air-saturated by bubbling air for 30 minutes. About 40 mL of electrolyte was used for each test.

The OCP (open circuit potential) measurement was performed monitoring the potential of the sample (WE) in the 3.5 wt.% NaCl solution versus the reference electrode (RE) for 1 hour.

Potentiodynamic anodic polarization studies were carried out by scanning the potential +1.0 V from the OCP value. Tafel plots were obtained by scanning the potential from -0.25 V to +0.25 V from OCP. LPR plots were obtained by scanning the potential from -0.02 V to +0.02 V from OCP. All tests were carried out with a scan rate of 0.16 mV/s.

EIS measurements were carried out by applying a small amplitude voltage of 10 mV (single sine wave

type) to the previously determined OCP value. The frequency ranged from 10 kHz to 1 mHz. The number of frequencies was 50.

All potentials from experimental data were converted to the saturated calomel electrode (SCE) scale to facilitate the discussion.

3 Results and discussion

The nickel-phosphorus and nickel-phosphorus-SiC coatings obtained from electroless plating process were classified according to the baths employed for their synthesis. The used nomenclature of the samples is summarized in *Table 1*.

Tab. 1: Classification of electroless Ni-P/ Ni-P SiC deposits

	Ni-P deposits	*Ni-P-SiC deposits*
Lab made baths	S1	C1
Commercial baths	S2	C2

3.1 Morphology

The scanning electron micrographs of the deposits are shown in *Figure 1*. For both nickel-phosphorus deposits S1 (a) and S2 (c), a regular, continuous and relatively smooth morphology is observed. Deposit S2 (c) shows the presence of micro-pores uniformly distributed over the surface. Cross sectional views also confirmed the presence of pores. In the case of the nickel-phosphorus-SiC composite deposits C1 (b) and C2 (d), a coarse morphology with uniform distribution of SiC particles can be observed. There are neither conglomerated nor depleted zones of particles. The incorporation of dispersed SiC microparticles seems to prevent the growth of pores.

3.2 Chemical composition

Figure 2 shows a comparison of the average results of chemical analysis carried out by GD-OES. It can be seen that composite deposits have similar content of incorporated SiC microparticles: deposit C1 with 9.4 wt% SiC and deposit C2 with 11.4 wt% SiC. All deposits are considered to be high phosphorus coatings [1].

Since microstructure, corrosion behavior and other properties are depending on the phosphorus content in nickel-phosphorus deposits [1], a detailed description of the phosphorus content across the thickness of the deposits can be seen in *Figure 3*. In this case, for the evaluation of the phosphorus content of the nickel-phosphorus alloy (or nickel-phosphorus alloy matrix in the case of C1 and C2), only nickel and phosphorus were considered (without regarding the particles in the case of composite deposits).

Comparing the phosphorus content as depth-profile analysis of all deposits (*Fig. 3*), it can be seen that

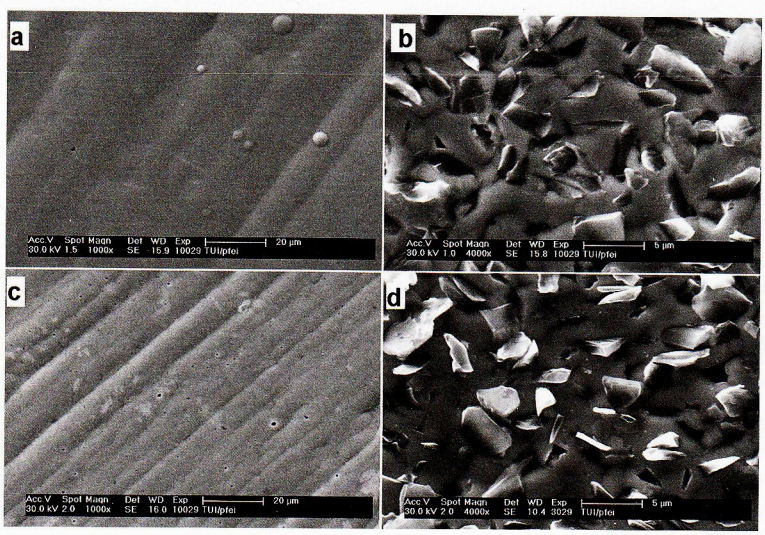

Fig. 1: SEM micrographs in top view of Ni-P and Ni-P-SiC deposits: a) S1 (1000x), b) C1 (4000x), c) S2 (1000x) and d) C2 (4000x)

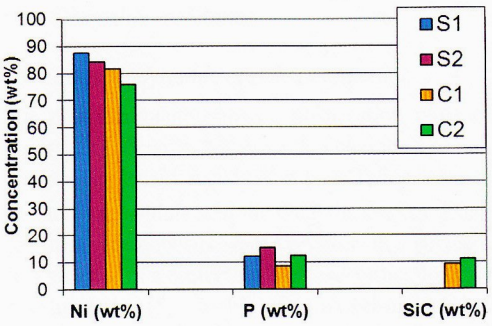

Fig. 2: Average results from GD-OES chemical analysis of deposits S1, S2, C1 and C2

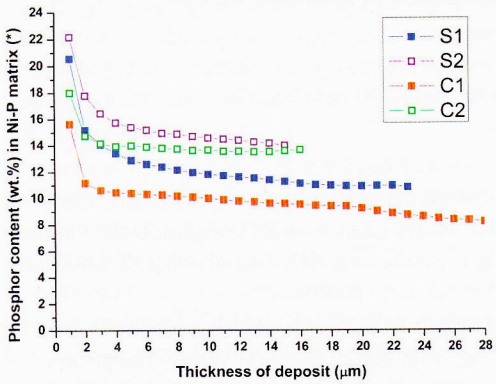

Fig. 3: Phosphorous content in Ni-P matrix of deposits as depth-profile analysis; (*) only nickel and phosphorous (100 %) were considered

the phosphorus content is not uniform across the thickness. At the surface, the phosphorus contents are higher than in the bulk. This is due to the slight decrease of the pH values of the baths during the plating process. Deposits resulting from commercial baths (S2 and C2) have higher phosphorus content because these baths also contained a higher quantity of hypophosphite (0.27 M) in comparison to lab made baths (0.18 M). On the other hand, by comparing the phosphorus content of the nickel-phosphorus deposits (S1 and S2) with their analogous composites (C1 and C2), it can be seen that phosphorus contents in composite deposits are lower than those of the pristine deposits. Thus, the presence of SiC particles seems to affect the phosphorus content of the nickel-phosphorus matrix of the composite deposits. Other works about electroless nickel with SiC and TiO_2 particles also reported this observation [8, 9].

The SiC content of the composite deposits C1 and C2 across their thickness can be considered constant. This means that SiC particles are well distributed in the metal matrix. *Figure 4a* shows the GD-OES depth-profile analysis for deposit C1 and *Figure 4b* shows a SEM micrograph of deposit C1 in cross sectional view showing the uniform distribution of particles as well.

3.3 Microstructure

The X-ray diffraction patterns of the as-deposited nickel-phosphorus and nickel-phosphorus-SiC coatings are shown in *Figure 5*. All XRD patterns have a common broad diffraction peak at the wide angular range of approx. 40° to 50° (2θ), those broad peaks were located around the 44.5° (2θ) position corresponding to the (111) diffraction peak of nickel. That indicates the amorphous character of the nickel-phosphorus matrix of the four deposits [1, 2, 10].

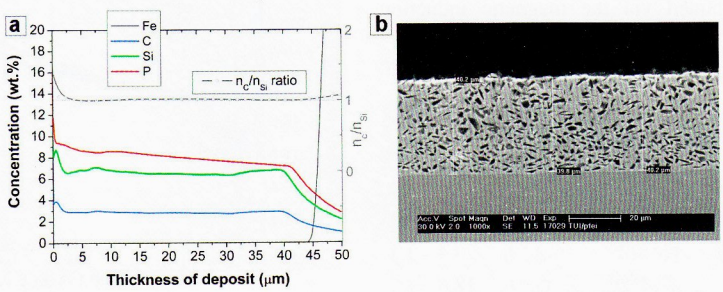

Fig. 4: SiC particle content distribution on deposit C1: a) detailed depth profile analysis by GD-OES, b) SEM micrograph in cross sectional view (1000x)

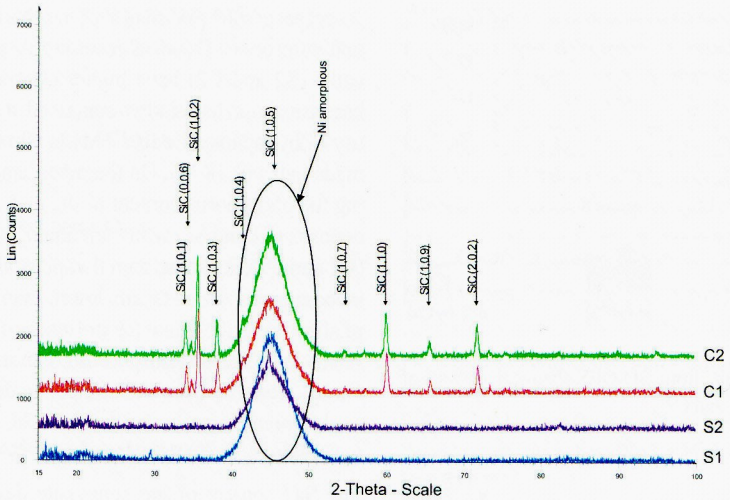

Fig. 5: XRD patterns of Ni-P and Ni-P-SiC coatings: S1, S2, C1 and C2

With a higher phosphorus content in the coating, the disorder of the nickel structure will also be higher and the structure becomes amorphous [11]. GD-OES analysis had shown that all deposits have high phosphorus contents, especially near the surfaces. Hence, these high phosphorus contents have influenced on the distortion of the lattice of nickel and resulted in amorphous structures of the deposits. Additionally, X-ray diffraction patterns of composite deposits C1 and C2 show some well-defined peaks corresponding to the crystal lattices of the 6H-SiC hexagonal polytype micro-particles.

3.4 Thickness of the deposits

Table 2 compares the thicknesses obtained by the magnetic induction method and SEM, respectively. The values obtained via the magnetic induction method represent average values; on the other hand, the values taken from SEM represent the thickness in a specific zone. The data infer that all the deposits have uniform thicknesses.

Deposits S1 and C1 (from lab made baths) were the ones with higher thickness values. The presence of particles in the plating baths had an influence on the deposition rate of the deposits. No clear relationship was found since by comparing deposits S1 and C1, the deposition rate of deposit C1 was higher and, on the other hand, by comparing deposits S2 and C2, the deposition rate of deposit C2 was lower.

Tab. 2: Thickness of deposits

Sample	*Thickness (µm)*	
	Magnetic induction method	*SEM*
S1	29	29.4
S2	20	18.6
C1	37	40.0
C2	16	16.6

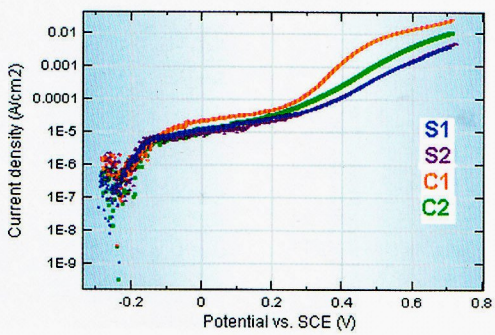

Fig. 6: Anodic polarization curves of deposits in 3.5 wt.% NaCl

4 Corrosion resistance

4.1 Potentiodynamic anodic polarization

The potentiodynamic anodic polarization plots of deposits in 3.5 wt.% NaCl are depicted in *Figure 6*. The current density is plotted in logarithmic scale.

At anodic potentials near the OCP the current densities of all the deposits were very low, this suggests the existence of a protective layer. According to other investigations [5, 12–14], for nickel-phosphorus deposits with high phosphorus content, a preferential dissolution of nickel occurs near the OCP leading to the enrichment of phosphorus on the surface layer. *Balaraju* et al. [5] reported that the barrier-action of the phosphorus enriched surface layer is related to the reaction of such layer with water to form a layer of adsorbed hypophosphite anions. This layer in turn would block the supply of water to the surface avoiding its dissolution.

At potentials above 0.3 V vs. SCE the current density increased quickly, which suggests that all deposits began to dissolve faster since, at high polarization conditions, the protective layer dissolves and nickel is oxidized to Ni^{2+} and Ni^{3+}. Deposit C1 is the one which experienced the highest dissolution current; this could be attributed to the lower phosphorus content in the bulk nickel-phosphorus matrix in comparison with the other samples.

After the anodic polarization test, pits were observed in deposit S2. According to the morphology of deposits, the presence of micropores was found in deposit S2.

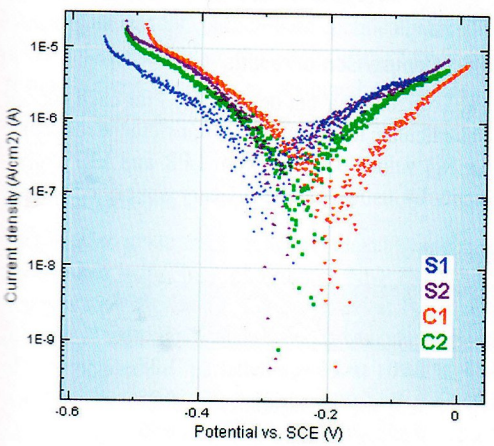

Fig. 7: Tafel plots of deposits in 3.5 wt.% NaCl

Thus, the occurrence of pits on deposit S2 (due to the reaction of the medium with the substrate) was expected. No pits were found on deposits S1, C1, and C2.

Special attention deserves the fact that the composite deposit C2 did not show presence of pits after anodic polarization in comparison to its analogous nickel-phosphorus deposit (S2). It can be concluded that the presence of dispersed SiC micro-particles prevented the growth of micro-pores during the deposition of C2.

4.2 Cathodic and anodic polarization

The Tafel plots are depicted in *Figure 7*. All deposits showed a Tafel behavior since the corrosion process is controlled by charge transfer over a wide potential range [15]. By extrapolating the linear portions of the polarization plots it was possible to calculate the electrochemical parameters (*Tab. 3*). Studies of EIS (see below) confirmed that charge transfer is the mechanistic pathway controlling the corrosion process of all deposits.

The composite deposits (C1 and C2) showed a lower corrosion current density (i_{corr}) than the simple deposits; among them, deposit C1 was the one with the lowest corrosion current density. The Stern-Geary

Tab. 3: Electrochemical parameters resulting from Tafel plots

Sample	*OCP vs. SCE (V)*	β_a *V/dec*	β_c *V/dec*	i_{corr} *µA/cm²*	*B (V)*
S1	-0.273	0.249	0.225	0.73	0.051
S2	-0.272	0.198	0.215	0.71	0.045
C1	-0.249	0.137	0.164	0.17	0.032
C2	-0.257	0.189	0.207	0.48	0.043

Tab. 4: Electrochemical parameters obtained from LPR

Sample	*OCP vs. SCE (V)*	*Rp (average) (Ω·cm²)*	*B (*) (V)*	i_{corr} *(**) (µA/cm²)*
S1	-0.264	49 693	0.051	1.03
S2	-0.258	55 501	0.045	0.80
C1	-0.246	103 611	0.032	0.31
C2	-0.267	77 954	0.043	0.55

(*) B values were calculated from Tafel slopes method
(**) i_{corr} values were calculated with the Stern-Geary simplified kinetic expression system [15]

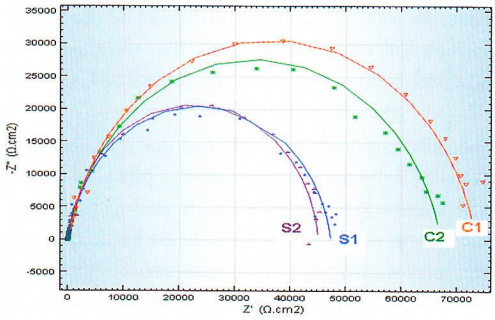

Fig. 8: Nyquist plots of deposits in 3.5 wt.% NaCl

constant (B) was calculated from the Tafel slopes values β_a and β_b for each system [15]. The electrochemical parameters obtained from LPR plots are described in *Table 4*. The composite nickel-phosphorus-SiC deposits showed the higher polarization resistance values (Rp).

4.3 Electrochemical impedance spectroscopy

The Nyquist plots (*Fig. 8*) of all deposits have, as a common feature, one big capacitive loop. That represents one time-constant on the impedance spectra and, in consequence, one reaction on the electrode/electrolyte interface responsible for the corrosion behavior of each sample. Thus, the charge transfer resistance (R_{ct}) is considered to be the electrochemical parameter that indicates the corrosion resistance of deposits. Thus, the charge transfer resistance can be identified as the polarization resistance (R_p).

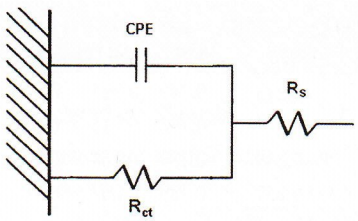

Fig. 9: Randles circuit

A Randles circuit (*Fig. 9*) was used to fit the data; this circuit simulates the electrochemical behavior of the Ni-P/Ni-P-SiC surface-solution interface. It contains elements corresponding to the solution resistance (R_s) placed in series with a circuit element composed of a charge transference resistance in parallel with a double-layer capacitance (C_{dl}). To model the double-layer capacitance, a constant phase element (CPE) was used instead of the double-layer capacitance. The use of a constant phase element is recommended in order to compensate the heterogeneity of the system [16]. In this case, an example of heterogeneity is the higher roughness of deposits C1 and C2 as a consequence of the presence of dispersed SiC microparticles. The constant phase element is defined by two parameters, Y_0 (admittance) and α (an empirical exponent related to the surface roughness). If α is equal to 1, the constant phase element is identical to a capacitor. Values of the double layer capacitance were calculated from the constant phase element parameters [14]. ω_{max} is the frequency of the maximum of Z'' (imaginary component of impedance).

Table 5 summarizes the electrochemical parameters obtained from EIS experiments. The values for charge transfer resistance of nickel-phosphorus-SiC composite deposits are higher than the ones obtained for nickel-phosphorus deposits. Charge transfer resistance (which is equal to R_p) and B values (which were calculated from Tafel slopes) were used for this calculation.

4.4 Comparison of results

The corrosion current density (i_{corr}) for each deposit was calculate using the charge transference resistance (or R_p) values obtained from LPR and EIS experiments by using the Stern-Geary simplified kinetic

Tab. 5: Electrochemical parameters obtained from EIS

Sample	*OCP vs. SCE (V)*	*R_s (Ωcm^2)*	*R_{ct} (Ωcm^2)*	*Y_0 (μS)*	*α*	*ω_{max} (Hz)*	*C_{dl} ($\mu F/cm^2$)*	*i_{corr} *) ($\mu A/cm^2$)*
S1	-0.258	11.7	47 687	3.13	0.90	0.24	18.0	1.08
S2	-0.278	11.4	46 729	3.90	0.95	0.16	21.4	0.95
C1	-0.271	12.8	71 001	3.80	0.89	0.13	24.0	0.46
C2	-0.246	12.5	66 047	4.29	0.89	0.09	28.2	0.65

*) icorr values were calculated with the Stern-Geary simplified kinetic expression [15]

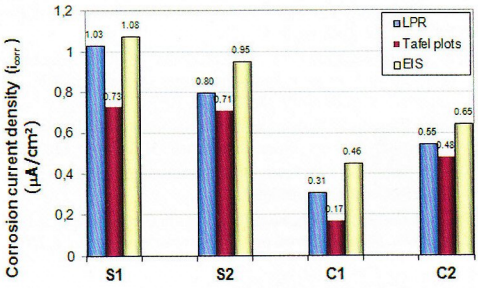

Fig. 10: Comparison of corrosion current density values obtained from LPR, EIS and Tafel plots

expression. Additionally, the corrosion current density (i_{corr}) of deposits was also obtained directly from the Tafel plots [15]. *Figure 10* depicts the corrosion current density values obtained from LPR, EIS and Tafel plots techniques.

According to *Figure 10*, the better corrosion behavior of the nickel-phosphorus-SiC composite deposits (C1 and C2) in comparison with nickel-phosphorus deposits (S1 and S2) is evident. The three electrochemical techniques used in this investigation confirm this behavior.

The characterization of nickel-phosphorus deposits (S1 and S2) and nickel-phosphorus matrices from composite deposits (C1 and C2) have demonstrated that their microstructure and chemical composition are similar. Then the behavior of these deposits in a corrosive environment is expected to be similar, the corrosion current densities obtained for this deposits confirm this fact. In the case of composite deposits, considering that SiC particles are chemically inert in a salt solution medium, the origin of the lower corrosion current densities is attributed to the lower available surface metallic area at the metal/solution interface.

5 Conclusions

By using lab made and commercial nickel/hypophosphite based baths, high phosphorus Ni-P /Ni-P-SiC deposits were obtained through an electroless plating process. In the case of composite deposits, the amount of incorporated SiC particles was about 10 wt.%.

All deposits showed an amorphous micro-structure and high phosphorus content. Depth profile analysis of deposits by GD-OES demonstrated that the phosphorus content of deposits is not uniform across their thickness. At the surface, the phosphorus contents were higher than in the bulk. This fact implies a phosphorus enrichment of the deposits.

Comparative studies of morphology (presence of pores) and examination of occurrence of pits (after anodic polarization tests) between deposits synthesized with commercial baths (S2 and C2) indicate that the presence of dispersed SiC micro-particles prevented the growth of micro-pores during the synthesis of C2.

The electrochemical methods (LPR, EIS, Tafel plots) used to study the corrosion resistance of nickel-phosphorus and nickel-phosphorus-SiC composite coatings in 3.5 wt.% NaCl solution showed that nickel-phosphorus-SiC composite coatings experience lower corrosion currents compared to the nickel-phosphorus coatings. This fact can be ascribed to the decrease in the effective area available for corrosion. Concerning to the mechanism by which the nickel-phosphorus and nickel-phosphorus-SiC become corroded, EIS experiments demonstrated that the corrosion process involved a charge transfer mechanism. Tafel plots also corroborated the charge transfer mechanism since all deposits showed a Tafel behavior in 3.5 wt.% NaCl solution.

Acknowledgements

The authors would like to express their appreciation to the financial support of the ISAP-DAAD exchange program and to the LUCET 90 Project L-004 granted to the "Instituto de Corrosión y Protección" of the "Pontificia Universidad Católica del Perú". The authors wish also to acknowledge Dipl.-Ing. M. Wilke, Dr.-Ing. K. Pfeifer and Dipl.-Ing. R. Grieseler for their valuable support in GD-OES, SEM and XRD measurements, respectively.

References

[1] G. O. Mallory: Electroless Plating: Fundamentals and Applications (Reprint Ed.); 1990, Noyes Publications, William Andrew Publishing, U.S.A.

[2] N. Kanani: Chemische Vernicklung: Nickel-Phosphor-Schichten Herstellung – Eigenschaften – Anwendungen, 2007, Eugen G. Leuze Verlag, Germany

[3] R. J. Davis: Nickel, cobalt and their alloys (1st Ed.); 2000, ASM International, U.S.A.

[4] J. N. Balaraju, T. S. N. Sankara, S. K. Seshadri: Electroless Ni-P composite coatings; Journal of Applied Electrochemistry, 33, 2003, pp. 807–816

[5] J. N. Balaraju, T. S. N. Sankara Narayanan, S. K. Seshadri: Evaluation of the corrosion resistance of electroless Ni-P and Ni-P composite coatings by electrochemical impedance spectroscopy; Journal of Solid State Electrochemistry, 5, 2001, pp. 334–338

[6] L. Spieß, G. Teichert, R. Schwarzer, H. Behnken, C. Genzel: Moderne Röntgenbeugung (2d Ed.); 2009, Vieweg+Teubner, Germany

[7] ASTM B 499 (2002) Standard Test Method for Measurement of Coating Thicknesses by the Magnetic Method: Nonmagnetic Coatings on Magnetic Basis Metals

[8] G. Jiaqiang, L. Lei, W. Yating, S. Bin, H. Wenbin: Electroless Ni–P–SiC composite coatings with superfine particles; Surf. Coat. Technol. 200 (20-21), 2006, 5836

[9] J. Novakovic, P. Vassiliou, Kl. Samara, Th. Argyropoulos: Electroless NiP–TiO2 composite coatings: Their production and properties; Surf. Coat. Technol. 201 (3-4), 2006, 895

[10] K. G. Keong, W. Sha, S. Malinov: Crystallisation kinetics and phase transformation behaviour of electroless nickel-phosphorus deposits with high phosphorus content; Journal of Alloys and Compounds, 334, 2002, pp. 192–199

[11] J. N. Balaraju, K. S. Rajam: Electroless Deposition and Characterization of High Phosphorus Ni-P-Si3N4 Composite Coatings; Int. J. Electrochem. Sci., 2, 2007, pp. 747–761

[12] F. Bigdeli, S. R. Allahkaram: The Corrosion Behaviour of Electroless Ni-P-SiC Nano-Composite Coating; International Journal of Modern Physics B, 22, 2008, pp. 3031–3036

[13] B. Elsener, M. Crobu, M. A. Scorciapino, A. Rossi: Electroless deposited Ni-P alloys: corrosion resistance mechanism; Journal of Applied Electrochemistry, 38, 2008, pp. 1053–1060

[14] A. Królikowski, B. Karbownicka, O. Jaklewicz: Anodic dissolution of amorphous Ni-P alloys; Electrochimica Acta, 51, 2006, pp. 6120–6127

[15] N. G. Thompson, J. H. Payer: DC Electrochemical Test Methods (1st Ed.); 1998, NACE International, U.S.A.

[16] G. S. Frankel: Electrochemical Techniques in Corrosion: Status, Limitations, and Needs; Journal of ASTM International, 5, No. 2, 2008

Über alles reden, nicht alles sagen

Bei Mitarbeitergesprächen und Teamsitzungen regiert vielfach Vorsicht und Rücksicht. Das ist gut so, wenn trotzdem alle anstehenden Themen offen und frei angesprochen werden. Angriffe auf die Persönlichkeit und die Privatheit der Teilnehmer haben in Geschäftsbesprechungen keinen Platz. Ebensowenig Platz sollten auch Phrasen haben, die jedes Gespräch töten. Dem ist aber nicht so.

Aussagen wie *das haben wir schon immer so gemacht* oder *das haben wir noch nie so gemacht* oder *das haben wir schon alles versucht*, belasten nicht nur das aktuelle Gesprächsklima, sondern haben bisweilen ungeahnte Folgewirkungen zum Nachteil der Firma. Ungezählte Killerphrasen, unbedacht dahingesagt, erzeugen Frust und Schweigsamkeit bei Mitarbeitern und Kollegen.

Die Frustrationstoleranz hat einen persönlichen Schwellenwert und richtet sich nach der persönlichen Situation und Persönlichkeit des Einzelnen. Ob diese Toleranzgrenze zeitlich befristet oder dauerhaft überschritten wird, äußert sich nicht offen erkennbar, sondern nur indirekt.

Killerphrasen schaden nicht nur dem Gesprächsklima, sondern machen den Gesprächspartner mundtot. In der Gruppe stellen sie ihn bloß und behindern damit das Weiterdenken, den kreativen Prozess und die Mitarbeit an Problemlösungen.

Da der Schaden – Opposition, kein Mitdenken mehr bis hin zur inneren Kündigung – sich nicht gleich einstellt, sondern schleichend, Zeit verzögert ankommt, wird er kaum wahrgenommen. Seriösen Schätzungen zufolge entgehen deutschen Firmen jährlich mehrere Millionen Euro nur dadurch, dass Mitarbeiter *ausgebremst* werden und daraus die Lehre ziehen, zukünftig nur noch das Notwendigste beizutragen.

Phrasen zu vermeiden und persönliche Kommunikationswege zu finden, die ein positives Klima schaffen und möglichst viele Betroffene zu Beteiligten machen, ist zentrale Aufgabe aller Führungsebenen. Gesprächstechniken, nicht umsonst als Techniken definiert, sind erlern- und übbar.

Eine kritische Eigenbeobachtung und ein Spiegelbild durch Außenstehende kann für Lernerfolge hilfreich sein. Neben einer offenen und authentischen Persönlichkeit tragen sie zum nachhaltigen Firmenerfolg bei. -dir-

Franz Sebl, Unternehmensberatung, Trappengasse 13a, A-8054 Graz